

Perceive-to-Reason: Decoupling Perception and Reasoning for Fine-Grained Visual Reasoning

Hongxing Li^{1,2,*}, Xiufeng Huang^{2,*}, Dingming Li¹, Wenjing Jiang^{1,2}, Zixuan Wang¹,
Haolei Xu^{1,2}, Hanrong Zhang², Haiwen Hong^{2,†}, Longtao Huang², Hui Xue²,
Weiming Lu¹, Jun Xiao¹, Yueting Zhuang¹, Yongliang Shen^{1,†}

¹Zhejiang University ²Alibaba Group



Abstract

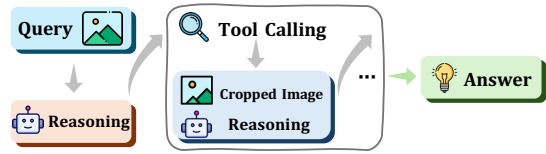
Fine-grained visual reasoning remains challenging for vision-language models, especially when small but critical visual cues are buried in high-resolution images. Existing approaches rely on repeated cropping or test-time visual search to introduce local evidence, but they typically do not explicitly distinguish perception from reasoning. In this paper, we propose **Perceive-to-Reason (P2R)**, a unified framework that formulates fine-grained visual reasoning as a two-stage process: the model first localizes question-relevant evidence as a *Perceiver*, and then answers the question as a *Reasoner* based on the annotated image and cropped regions. To better align training with this decoupled formulation, we further introduce **Perception-Reasoning Alternating GRPO (PRA-GRPO)**, a role-aware reinforcement learning strategy that alternates between perception-focused and reasoning-focused updates using only final-answer supervision. Built on top of Qwen3-VL-Instruct-2B/4B/8B, P2R consistently improves performance across model scales. In particular, P2R-4B achieves 93.2% on V-Star, 81.9% on HR-Bench-4K, and 80.5% on HR-Bench-8K, substantially outperforming its corresponding backbone. Further experiments show that the benefits of P2R extend beyond high-resolution benchmarks to broader multimodal reasoning tasks. These results suggest that explicitly decoupling perception from reasoning provides an effective framework for fine-grained visual reasoning.

1 Introduction

Vision-language models (VLMs) have recently achieved strong performance on general visual understanding and reasoning tasks (Huang et al., 2025; Yu et al., 2025a). Yet fine-grained visual reasoning remains challenging (Wu and Xie, 2024; Wang et al., 2025d; Zhang et al., 2024), especially for tasks such as fine-grained text recognition and precise spatial relation understanding. Solving

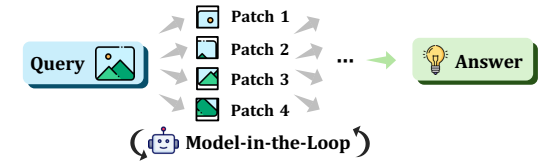
Thinking with Images (e.g. DeepEyes)

🔴 Noisy Context, Difficult to Attribute



Visual Search Methods (e.g. ZoomEye)

🔴 Complex Pipeline, Difficult to Optimize



Perceive-to-Reason (Ours)

🟢 Clean Context, Simple Pipeline, Easy to Optimize

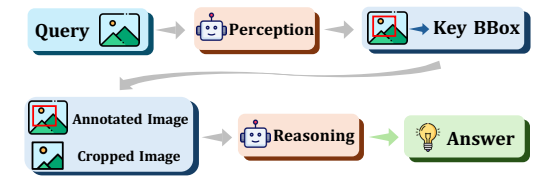


Figure 1: Motivation of P2R. Prior methods inject local evidence via cropping or search without explicitly separating perception and reasoning. P2R instead adopts a decoupled perceive-to-reason paradigm.

such tasks requires both locating subtle question-relevant evidence in high-resolution images and reasoning over it, that is, determining *where to look* and *how to reason*.

A simple diagnostic study suggests that perception is a major bottleneck in fine-grained visual reasoning. On V-Star (Wu and Xie, 2024), Qwen3-VL-Instruct-4B (Bai et al., 2025) improves from 81.7% to 90.6% when given oracle bounding boxes and cropped regions, indicating that many errors stem from failing to localize the right visual evidence (details in Appendix A).

Existing approaches mainly address this challenge by injecting local evidence through region cropping or search (Shao et al., 2024a; Liu et al.,

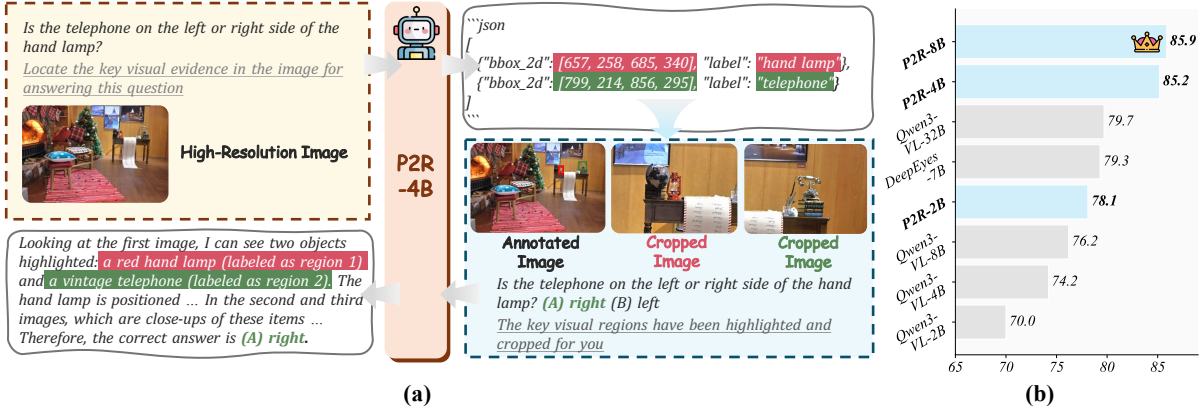


Figure 2: Overview of P2R. (a) Illustration of the proposed two-stage P2R inference pipeline. (b) Performance comparison on fine-grained visual reasoning benchmarks. P2R outperforms its base models across all scales.

2024). They largely fall into two categories. *Thinking with Images* methods (Zheng et al., 2025b; Wang et al., 2025c) interleave region exploration with reasoning, often producing long and noisy contexts. Visual search methods (Shen et al., 2025b; Li et al., 2025b) locate key regions through test-time search, but typically rely on complex pipelines that are difficult to optimize (Li et al., 2026; Liu et al., 2025b). More importantly, these approaches either entangle evidence localization with reasoning or externalize perception into a separate search process, so the model is not directly optimized for *where to look* decisions, as illustrated in Figure 1.

These observations motivate a two-stage formulation of fine-grained visual reasoning: first localize the relevant evidence, then reason over it. However, training such a decoupled process is difficult under answer-only supervision, since errors may arise from either poor localization or flawed reasoning, making credit assignment ambiguous.

To address this issue, we propose **Perceive-to-Reason (P2R)**, a unified framework that explicitly decomposes fine-grained visual reasoning into perception and reasoning. At inference time, P2R first localizes question-relevant evidence as a *Perceiver*, and then answers the question as a *Reasoner* based on the annotated image and cropped regions. This formulation makes evidence localization an explicit intermediate step rather than an implicit byproduct of answer generation.

To train this decoupled formulation, we further propose **Perception-Reasoning Alternating GRPO (PRA-GRPO)**, a role-aware reinforcement learning strategy built upon GRPO (Shao et al., 2024b). PRA-GRPO alternates between perception-focused and reasoning-focused optimization while keeping the other role fixed, thereby converting final-answer

correctness into a more attributable training signal for the active stage. In this way, P2R improves both evidence localization and answer generation using only final-answer supervision, without requiring ground-truth bounding box annotations.

Built on top of Qwen3-VL-Instruct (Bai et al., 2025), P2R consistently improves over its base models across all scales. In particular, P2R-4B achieves 93.2% on V-Star (Wu and Xie, 2024), 81.9% on HR-Bench-4K (Wang et al., 2025d), and 80.5% on HR-Bench-8K (Wang et al., 2025d), with substantial gains over the corresponding backbone. Further experiments show that the benefits of P2R extend beyond high-resolution benchmarks to broader multimodal reasoning tasks. Our main contributions are summarized as follows:

- We propose P2R, a unified framework for fine-grained visual reasoning that formulates the task as a two-stage perceive-to-reason process, explicitly decoupling evidence localization from answer generation.
- We introduce PRA-GRPO, a role-aware reinforcement learning strategy that aligns training with the decoupled perceive-to-reason formulation, using only final-answer supervision without requiring bounding box annotations.
- Built on top of Qwen3-VL-Instruct models, P2R consistently delivers substantial gains across model scales and achieves state-of-the-art results on high-resolution fine-grained visual reasoning benchmarks.

2 Related Work

Fine-Grained Visual Reasoning. Fine-grained visual reasoning requires models to identify subtle

visual evidence and reason over it, and remains challenging for current VLMs (Wu and Xie, 2024; Wang et al., 2025d; Zhang et al., 2024; Wei et al., 2026; Wang et al., 2025b; Li et al., 2025a). Existing methods mainly tackle this challenge by localizing key regions. One line of work follows the *Thinking with Images* paradigm (Hong et al., 2025; Lai et al., 2025; Fan et al., 2025; Wang et al., 2025a; Zhao et al., 2025, 2026), where models iteratively zoom into relevant regions or invoke visual tools for interleaved visual-textual reasoning. For example, DeepEyes (Zheng et al., 2025b) leverages reinforcement learning to improve visual tool use. Another line of work adopts visual search or test-time scaling (Yu et al., 2025b; Shao et al., 2024a; Khayatkhoei et al., 2025; Hu et al., 2024) to identify informative subregions during inference; for instance, ZoomEye (Shen et al., 2025b) performs hierarchical search over zoomed-in regions. However, these methods either entangle perception and reasoning within a single process or rely on external pipelines, without explicitly formulating fine-grained visual reasoning as a perceive-to-reason process. Our method, in contrast, explicitly decomposes the task and aligns training accordingly.

Reinforcement Learning in VLMs. Recent studies have extended reinforcement learning (RL) from LLMs to VLMs, leading to notable progress in visual reasoning (Yu et al., 2025a; Liu et al., 2025e; Yang et al., 2025; Li et al., 2025c; Wang et al., 2025e; Liu et al., 2025a,c; Chen et al., 2025; Wang et al., 2026). Representative works such as Vision-R1 (Huang et al., 2025) and MM-Eureka (Meng et al., 2025) show that RL can significantly improve reasoning capabilities in VLMs, especially for visual mathematical reasoning. Perception-oriented methods such as VLM-R1 (Shen et al., 2025a) and Perception-R1 (Yu et al., 2025a) use rewards based on IoU or F1 to improve grounding and counting. However, existing RL approaches optimize perception and reasoning in isolation, without addressing their coordination. Our PRA-GRPO instead optimizes both within a unified framework via alternating updates.

3 Methodology

3.1 P2R Framework Overview

P2R is a unified framework that formulates fine-grained visual reasoning as a perceive-to-reason process. It consists of two tightly coupled components: a two-stage inference paradigm that ex-

plicitly separates evidence localization and answer generation, assigning these roles to a *Perceiver* and a *Reasoner*, and PRA-GRPO, a role-aware reinforcement learning strategy that aligns training with this decoupled formulation.

3.2 Two-Stage P2R Inference

Given an image-question pair (I, Q) , P2R structures fine-grained visual reasoning into two consecutive stages: perception and reasoning, as illustrated in Figure 2(a). We use a single underlying VLM with shared parameters θ throughout both stages. For notational convenience, we denote its role-conditioned behavior in the perception and reasoning stages as $\pi_p(\cdot; \theta)$ and $\pi_r(\cdot; \theta)$, corresponding to the *Perceiver* and *Reasoner*, respectively.

In the first stage, the model acts as a *Perceiver* to make an explicit localization decision for the visual evidence most relevant to answering the question. Let $\tilde{Q}_p = \mathcal{T}_p(Q)$ denote a perception-oriented prompt derived from the original question. The *Perceiver* predicts one or more bounding boxes as:

$$\mathcal{B} \sim \pi_p(\cdot \mid I, \tilde{Q}_p; \theta) \quad (1)$$

where $\mathcal{B} = \{B_k\}_{k=1}^K$ denotes a set of rectangular regions in the image, and each $B_k = (x_1, y_1, x_2, y_2)$ specifies one region.

The predicted boxes are then transformed into two complementary visual inputs: an annotated image $I_a = \text{annotate}(I, \mathcal{B})$ and cropped evidence images $I_c = \text{crop}(I, \mathcal{B})$, where $\text{annotate}(\cdot)$ overlays the predicted boxes on the original image and $\text{crop}(\cdot)$ extracts the corresponding local regions.

In the second stage, the model acts as a *Reasoner* and generates the final answer as:

$$Y \sim \pi_r(\cdot \mid I_a, I_c, Q; \theta) \quad (2)$$

This two-stage formulation turns fine-grained visual reasoning into an explicitly structured process: the *Perceiver* determines *where to look*, while the *Reasoner* focuses on *how to reason* from the evidence. By making evidence localization an explicit intermediate step rather than an implicit byproduct of answer generation, P2R offers a more suitable formulation for fine-grained visual reasoning.

3.3 PRA-GRPO

Training the Decoupled Formulation. While the two-stage P2R inference process explicitly separates perception from reasoning, training remains challenging because the final prediction depends

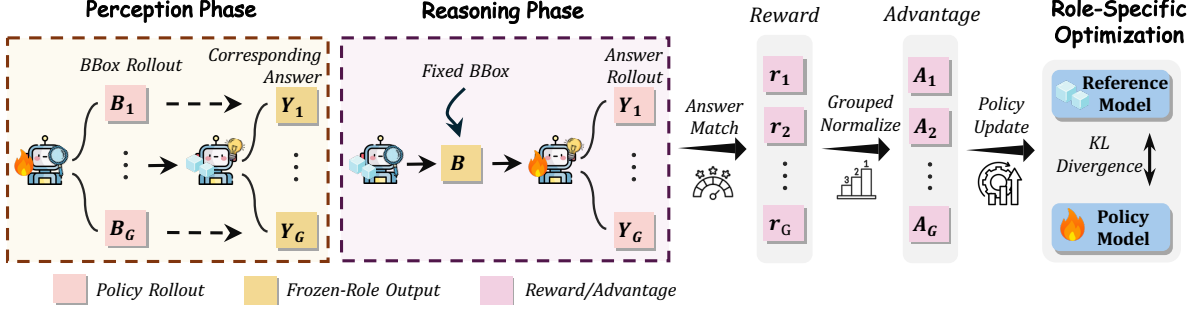


Figure 3: Overview of PRA-GRPO. Training alternates between a perception phase and a reasoning phase under shared model parameters. In each phase, the active role is optimized with GRPO while the other role is frozen, so that final answer correctness can be converted into a more attributable role-specific learning signal.

on both stages. Incorrect evidence localization can mislead downstream reasoning, while correct evidence alone does not guarantee a correct answer if the subsequent reasoning is still flawed. As a result, it is difficult to improve fine-grained visual reasoning by treating the entire pipeline as a single undifferentiated optimization problem. Since supervision is only available at the level of the final answer, it is difficult to determine how the learning signal should be attributed across the two stages, especially when perception must be learned from downstream reasoning outcomes alone.

Role-Aware Alternating Optimization. To address this issue, we propose PRA-GRPO, a role-aware reinforcement learning strategy that aligns optimization with the perceive-to-reason structure of P2R, as illustrated in Figure 3. The key idea is to convert final answer correctness into a more attributable training signal by alternating perception-focused and reasoning-focused updates. Intuitively, better evidence localization should increase the likelihood of successful downstream reasoning; therefore, even without ground-truth bounding box annotations, the final answer can serve as an indirect supervision signal for learning perception.

Concretely, PRA-GRPO alternates between optimizing the *Perceiver* and the *Reasoner*, while keeping the other role fixed. This turns final answer correctness into a role-aware supervision signal: in the perception phase, the quality of the predicted evidence is evaluated through the answer produced by a fixed *Reasoner*; in the reasoning phase, answer generation is optimized conditioned on evidence provided by a fixed *Perceiver*.

We now formalize this role-aware alternating optimization under the GRPO framework. Given an image-question-answer triplet (I, Q, Y) , we sample a group of G rollouts from the role currently

being optimized. In the perception phase, o_i is a set of bounding boxes $\mathcal{B}_i \sim \pi_p(\cdot | I, \mathcal{T}_p(Q); \theta)$. Based on \mathcal{B}_i , we construct the annotated image I_a^i and cropped evidence images I_c^i , which are then fed into a fixed *Reasoner* to obtain the final answer Y_i . In the reasoning phase, o_i is an answer $Y_i \sim \pi_r(\cdot | I_a, I_c, Q; \theta)$, where (I_a, I_c) are constructed from the bounding boxes predicted by the fixed *Perceiver*.

To keep supervision minimal and task-agnostic, we define a binary reward based solely on final-answer correctness:

$$r_i = \mathbb{I}[Y_i = Y] \quad (3)$$

where $\mathbb{I}[\cdot]$ is the indicator function.

Role-Aware GRPO Objective. We compute the group-relative advantage following GRPO (Shao et al., 2024b; Guo et al., 2025):

$$A_i = \frac{r_i - \text{mean}(\{r_j\}_{j=1}^G)}{\text{std}(\{r_j\}_{j=1}^G) + \epsilon} \quad (4)$$

where ϵ is a small constant for numerical stability. We then optimize the active role in the current phase using the standard GRPO objective:

$$\mathcal{J}_{\text{GRPO}}^\phi(\theta) = \mathbb{E}_{x, \{o_i\}_{i=1}^G} \left[\frac{1}{G} \sum_{i=1}^G \min \left(\rho_i A_i, \text{clip}(\rho_i, 1 \pm \epsilon) A_i \right) - \beta \text{KL}[\pi_{\phi, \theta} \| \pi_{\text{ref}}] \right] \quad (5)$$

where

$$\rho_i = \frac{\pi_{\phi, \theta}(o_i | x)}{\pi_{\phi, \theta_{\text{old}}}(o_i | x)} \quad (6)$$

and $\phi \in \{p, r\}$ denotes the active role in the current optimization phase. Specifically, $x = (I, \mathcal{T}_p(Q))$ and $o_i = \mathcal{B}_i$ in the perception phase, while $x = (I_a, I_c, Q)$ and $o_i = Y_i$ in the reasoning phase.

Method	V-Star			HR-Bench-4K			HR-Bench-8K			Avg.
	Attr	Spatial	Overall	FSP	FCP	Overall	FSP	FCP	Overall	
Visual General Models										
GPT-4o (Hurst et al., 2024)	-	-	66.0	70.0	48.0	59.0	62.0	49.0	55.0	60.0
o3 OpenAI (OpenAI, 2025)	-	-	95.7	-	-	-	-	-	-	-
Qwen3-VL-Instruct-2B (Bai et al., 2025)	73.0	77.6	74.9	81.0	59.8	70.4	70.8	58.5	64.6	70.0
Qwen3-VL-Instruct-4B (Bai et al., 2025)	79.1	85.5	81.7	81.8	66.0	73.8	73.8	60.3	67.0	74.2
Qwen3-VL-Instruct-8B (Bai et al., 2025)	84.3	82.9	83.8	81.0	68.5	74.8	73.3	<u>70.1</u>	70.1	76.2
Qwen3-VL-Instruct-32B (Bai et al., 2025)	86.1	88.2	86.9	86.0	<u>71.3</u>	78.6	78.8	<u>68.5</u>	73.6	79.7
Visual Search Methods										
DyFo-7B (Li et al., 2025b)	80.0	82.9	81.2	-	-	-	-	-	-	-
ZoomEye-7B (Shen et al., 2025b)	93.9	85.5	90.6	84.3	55.0	69.6	88.5	50.0	69.3	76.5
Thinking with Images Methods										
DeepEyes-7B (Zheng et al., 2025b)	91.3	88.2	90.1	91.3	59.0	75.1	86.8	58.5	72.6	79.3
PixelReasoner-7B (Wang et al., 2025c)	83.5	76.3	80.6	86.0	60.3	72.9	80.0	54.3	66.9	73.5
Thyme-7B (Zhang et al., 2025)	83.5	80.3	82.2	91.0	63.0	77.0	86.5	57.5	72.0	77.1
P2R (Ours)										
P2R-2B	84.3	84.2	84.3	89.8	60.1	75.1	86.8	62.7	74.8	78.1
Δ (vs Qwen3-VL-Instruct-2B)	<u>+11.3</u>	<u>+6.6</u>	<u>+9.4</u>	<u>+8.8</u>	<u>+0.3</u>	<u>+4.7</u>	<u>+16.0</u>	<u>+4.2</u>	<u>+10.2</u>	<u>+8.1</u>
P2R-4B	92.2	94.7	93.2	92.3	71.5	81.9	92.0	69.0	80.5	85.2
Δ (vs Qwen3-VL-Instruct-4B)	<u>+13.1</u>	<u>+9.2</u>	<u>+11.5</u>	<u>+10.5</u>	<u>+5.5</u>	<u>+8.1</u>	<u>+18.2</u>	<u>+8.7</u>	<u>+13.5</u>	<u>+11.0</u>
P2R-8B	<u>92.2</u>	96.1	93.7	93.5	71.5	<u>81.5</u>	94.5	70.8	82.6	85.9
Δ (vs Qwen3-VL-Instruct-8B)	<u>+7.9</u>	<u>+13.2</u>	<u>+9.9</u>	<u>+12.5</u>	<u>+3.0</u>	<u>+6.7</u>	<u>+21.2</u>	<u>+0.7</u>	<u>+12.5</u>	<u>+9.7</u>

Table 1: Quantitative results on V-Star, HR-Bench-4K, and HR-Bench-8K benchmarks. **Bold** denotes the best and underline denotes the second best.

As both roles are instantiated by the same underlying VLM with shared parameters θ , PRA-GRPO improves both evidence localization and answer generation within a unified model. More importantly, it allows perception to be learned from downstream reasoning outcomes through final-answer supervision alone, without requiring ground-truth bounding boxes or task-specific dense rewards.

See Appendix B for more method details.

4 Experiments

4.1 Experimental Setup

Baselines and Benchmarks. We compare P2R against three groups of representative baselines: (1) general-purpose VLMs, including proprietary models such as GPT-4o (Hurst et al., 2024) and o3 (OpenAI, 2025), as well as open-source Qwen3-VL (Bai et al., 2025) models of different sizes; (2) visual search methods, including DyFo (Li et al., 2025b) and ZoomEye (Shen et al., 2025b); and (3) thinking-with-images methods, including DeepEyes (Zheng et al., 2025b), PixelReasoner (Wang et al., 2025c), and Thyme (Zhang et al., 2025). Our primary evaluation targets high-resolution fine-grained visual reasoning benchmarks, including V-Star (Wu and Xie, 2024) and HR-Bench (Wang et al., 2025d), which require precise perception of subtle visual evidence followed by downstream reasoning. We further report results on MME-RealWorld-Lite (Zhang et al., 2024) to assess whether the benefits of P2R extend to broader real-world multimodal reasoning scenarios.

Training Dataset. We build a 10K training set by sampling 3K examples from DeepEyes (Zheng et al., 2025b), 3K from VisualProbe (Lai et al., 2025), and 4K from ZwZ (Wei et al., 2026).

Training Details. We instantiate P2R on top of Qwen3-VL-Instruct (Bai et al., 2025) models using GRPO (Shao et al., 2024b) on 4 H100 GPUs. In each alternating stage, the Perceiver phase and the Reasoner phase are each trained for one epoch. For each prompt, we sample 8 rollouts, and set the KL coefficient (Kullback, 1951) to 0.01.

See Appendix C and D for more details.

4.2 Main Results

High-Resolution Benchmarks. Table 1 reports the results on V-Star (Wu and Xie, 2024), HR-Bench-4K (Wang et al., 2025d), and HR-Bench-8K (Wang et al., 2025d). P2R consistently outperforms its corresponding Qwen3-VL-Instruct baselines across all scales, indicating that the proposed perceive-to-reason formulation is effective for fine-grained visual reasoning. Averaged over the three benchmarks, P2R-2B, P2R-4B, and P2R-8B improve upon their Qwen3-VL-Instruct counterparts by 8.1%, 11.0%, and 9.7%, respectively. The gains are especially pronounced on HR-Bench-8K, highlighting the advantage of P2R in challenging high-resolution settings. P2R also compares favorably with prior visual search and thinking-with-images methods, with P2R-8B achieving the best average performance among all open-source models. A summary comparison is also shown in Figure 2 (b).

Method	Overall	Perception					Reasoning			
		OCR	RS	DT	MO	AD	OCR	DT	MO	AD
Qwen3-VL-Instruct-2B (Bai et al., 2025)	47.3	85.2	38.7	74.0	32.9	39.1	69.0	67.0	40.7	30.8
Qwen3-VL-Instruct-4B (Bai et al., 2025)	47.7	88.0	38.0	80.0	34.8	33.7	74.0	77.0	34.7	31.8
Qwen3-VL-Instruct-8B (Bai et al., 2025)	50.4	88.8	49.3	85.0	36.4	33.1	<u>81.0</u>	79.0	38.7	34.3
Qwen3-VL-Instruct-32B (Bai et al., 2025)	52.3	86.8	50.0	89.0	38.6	36.0	82.0	88.0	44.0	34.5
DeepEyes-7B (Zheng et al., 2025b)	53.2	<u>90.0</u>	<u>52.7</u>	89.0	43.3	33.4	76.0	69.0	44.0	35.0
PixelReasoner-7B (Wang et al., 2025c)	49.7	89.6	52.0	<u>86.0</u>	38.9	30.9	71.0	72.0	<u>46.0</u>	32.5
P2R-2B	51.3	88.4	43.3	78.0	39.8	<u>40.6</u>	76.0	68.0	44.0	35.5
Δ (vs Qwen3-VL-Instruct-2B)	<i>+4.0</i>	<i>+3.2</i>	<i>+4.6</i>	<i>+4.0</i>	<i>+6.9</i>	<i>+1.5</i>	<i>+7.0</i>	<i>+1.0</i>	<i>+3.3</i>	<i>+4.7</i>
P2R-4B	<u>54.8</u>	88.8	50.0	<u>86.0</u>	46.1	39.1	79.0	78.0	46.7	39.5
Δ (vs Qwen3-VL-Instruct-4B)	<i>+7.1</i>	<i>+0.8</i>	<i>+12.0</i>	<i>+6.0</i>	<i>+11.3</i>	<i>+5.4</i>	<i>+5.0</i>	<i>+1.0</i>	<i>+12.0</i>	<i>+7.7</i>
P2R-8B	57.4	92.4	58.7	89.0	<u>44.5</u>	46.9	<u>81.0</u>	<u>81.0</u>	46.7	<u>39.0</u>
Δ (vs Qwen3-VL-Instruct-8B)	<i>+7.0</i>	<i>+3.6</i>	<i>+9.4</i>	<i>+4.0</i>	<i>+8.1</i>	<i>+13.8</i>	<i>+0.0</i>	<i>+2.0</i>	<i>+8.0</i>	<i>+4.7</i>

Table 2: Quantitative results on MME-RealWorld-Lite benchmark. **Bold** denotes the best and underline denotes the second best among all methods.

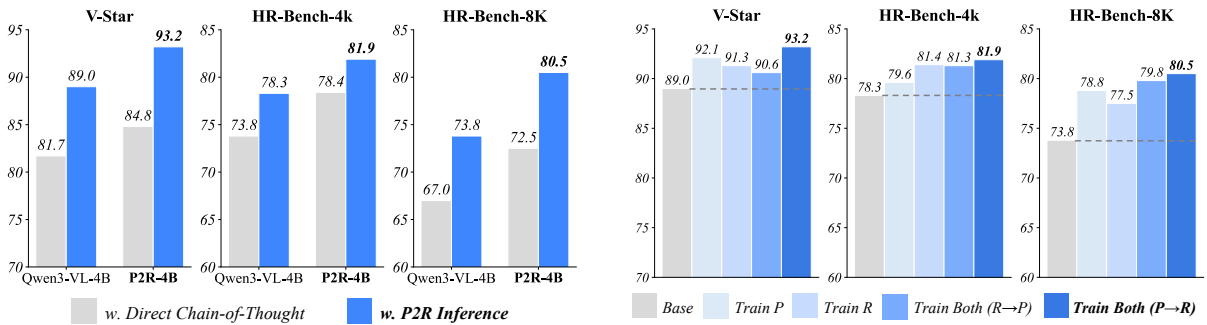


Figure 4: Comparison between direct CoT and P2R inference on Qwen3-VL-Instruct-4B and P2R-4B.

General Perception and Reasoning Benchmark.

Table 2 reports the results on MME-RealWorld-Lite (Zhang et al., 2024), a broad benchmark covering diverse real-world multimodal perception and reasoning tasks. P2R consistently improves over its Qwen3-VL-Instruct backbones, with overall gains of 4.0%, 7.1%, and 7.0% for the 2B, 4B, and 8B models, respectively. Notably, these improvements are broad rather than concentrated in a few categories: P2R improves performance across nearly all sub-tasks in both perception and reasoning. This suggests that the benefits of the perceive-to-reason formulation extend beyond high-resolution fine-grained settings to more general multimodal understanding scenarios. P2R-8B achieves the best overall performance among all compared methods.

4.3 Ablation Study

Effect of P2R Inference. Figure 4 compares direct chain-of-thought (Wei et al., 2022) prompting with the proposed P2R inference on both Qwen3-VL-Instruct-4B and P2R-4B. P2R inference consistently improves performance across all three benchmarks for both models, suggesting that the perceive-to-reason decomposition is beneficial already at inference time. On V-Star, for example,

Figure 5: Ablation of PRA-GRPO training components on Qwen3-VL-Instruct-4B. *Train P* and *Train R* optimize only the perceiver or the reasoner; *Train Both* alternates between the two roles. The dashed line denotes the Qwen3-VL-4B baseline with P2R inference.

replacing direct CoT with P2R inference improves the score from 81.7% to 89.0% for Qwen3-VL-Instruct-4B, and from 84.8% to 93.2% for P2R-4B. Moreover, P2R-4B remains stronger than Qwen3-VL-Instruct-4B even under direct CoT prompting, indicating that the benefits of PRA-GRPO are not limited to the dedicated P2R inference pipeline. Combining P2R training with P2R inference yields the strongest performance on all three benchmarks.

Effect of PRA-GRPO Training. Figure 5 compares different PRA-GRPO training strategies on top of Qwen3-VL-Instruct-4B with P2R inference. Optimizing either role alone already improves over the no-training baseline, suggesting that both perception and reasoning can benefit from role-aware training. Alternating updates over both roles leads to further gains across benchmarks. On V-Star, the order $P \rightarrow R$ achieves 93.2%, outperforming $R \rightarrow P$ at 90.6%, suggesting that localizing evidence first better supports reasoning by providing more accurate visual inputs. These results support the effectiveness of aligning training with the decoupled perceive-to-reason formulation.

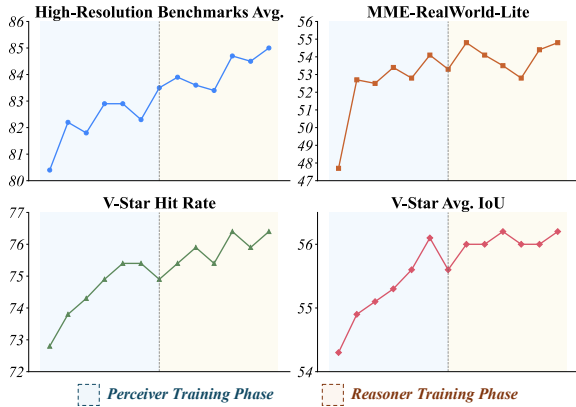


Figure 6: Training dynamics of PRA-GRPO during the Perceiver and Reasoner training phases.

P Ckpt	R Ckpt	V-Star	HR-4K	HR-8K	Avg.
<i>Base</i>	<i>Base</i>	89.0	78.3	73.8	80.4
<i>P-Only</i>	<i>Base</i>	90.6	78.6	78.1	82.4
<i>P-Only</i>	<i>P-Only</i>	92.1	79.6	78.8	83.5
<i>Base</i>	<i>R-Only</i>	90.8	80.5	76.9	82.7
<i>R-Only</i>	<i>R-Only</i>	91.3	81.4	77.5	83.4
<i>P-Only</i>	<i>R-Only</i>	92.1	81.4	81.0	84.8
<i>P2R-Full</i>	<i>P2R-Full</i>	93.2	81.9	80.5	85.2

■ Worst ■ ■ ■ Best

Table 3: Shared-parameter analysis using different perceiver and reasoner checkpoints on three fine-grained visual reasoning benchmarks. *Base* is the original model, *P-Only* and *R-Only* are checkpoints trained only for the perceiver or reasoner role, and *P2R-Full* is the final checkpoint after full PRA-GRPO training.

4.4 Further Analysis

Training Dynamics Figure 6 shows the training dynamics of PRA-GRPO. During the *Perceiver* phase, both V-Star Hit Rate and Avg. IoU improve steadily, indicating more accurate localization of question-relevant evidence. We define Hit Rate as 1 if the center of a predicted box falls inside the ground-truth box, making it a simple proxy for localization. Performance on the high-resolution benchmark average and MME-RealWorld-Lite also improves in this phase. After switching to the *Reasoner* phase, benchmark performance continues to increase while the localization metrics remain stable or improve slightly, suggesting complementary gains from the two roles. More training dynamics are provided in Appendix E.1.

Shared-Parameter Analysis. To study the effect of parameter sharing, we initialize the *Perceiver* and *Reasoner* in P2R inference with different checkpoints, including the base model, the *P-Only* and *R-Only* checkpoints, and the final PRA-

GRPO checkpoint, and evaluate their combinations on three fine-grained visual reasoning benchmarks.

Table 3 reveals clear cross-role transfer under shared parameters. Replacing the *Base Reasoner* with the *P-Only* checkpoint improves the average score from 82.4% to 83.5% (*P-Only* + *Base* vs. *P-Only* + *P-Only*), indicating that *Perceiver*-only training also benefits the model when reused in the *Reasoner* role. Likewise, replacing the *Base Perceiver* with the *R-Only* checkpoint increases the average score from 82.7% to 83.4% (*Base* + *R-Only* vs. *R-Only* + *R-Only*), suggesting that *Reasoner*-only training also transfers to the *Perceiver* role. However, simply combining separately trained checkpoints remains weaker than the final alternating model (84.8% vs. 85.2%), suggesting that PRA-GRPO better integrates both capabilities within a single shared model. In addition, this shared-parameter design is deployment-friendly, requiring only one model at inference time.

Method	Acc@0.5 _{test}	Acc@0.5 _{val}	Avg.
Qwen3-VL-4B	59.1	64.1	61.6
P2R-4B	59.6	65.9	62.7
Δ	+0.5	+1.8	+1.1

Table 4: Grounding Generalization on ReasonSeg

Generalization to Grounding Tasks. We further evaluate P2R-4B on the reasoning grounding task in ReasonSeg (Lai et al., 2024) to assess whether PRA-GRPO transfers to localization tasks that require reasoning over the query. As shown in Table 4, P2R-4B consistently outperforms Qwen3-VL-Instruct-4B on both the test and validation splits, improving Acc@0.5 by 0.5% and 1.8%, respectively, for an average gain of 1.1%.

Notably, P2R is trained without any grounding-specific data or ground-truth bounding box annotations, relying only on final-answer supervision from fine-grained visual reasoning data. This suggests that the improvements induced by PRA-GRPO transfer beyond the original training setup and can enhance localization of query-relevant visual evidence in downstream grounding tasks.

Training Scaling Analysis. Figure 8 shows the performance growth of PRA-GRPO and text-only GRPO over three training iterations on MME-RealWorld-Lite. While both methods improve with additional training, PRA-GRPO scales faster, rising from 54.8% to 57.1% with a fitted slope of 0.77, compared with 53.8% to 55.1% and a slope of 0.43 for text-only GRPO.

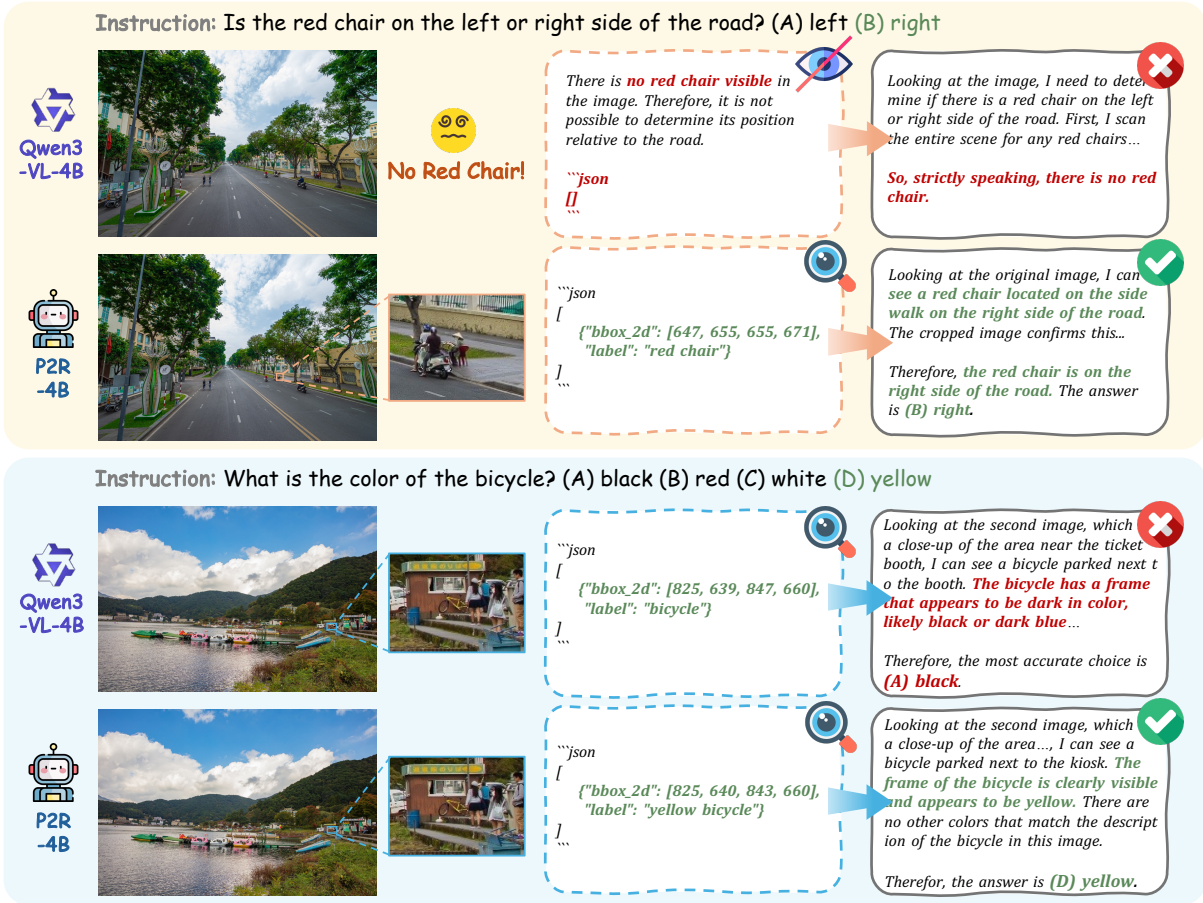


Figure 7: Representative examples from the V-Star benchmark, comparing Qwen3-VL-4B and P2R-4B.

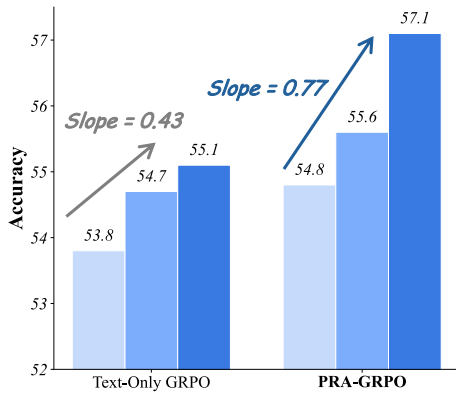


Figure 8: Performance over three iterations on MME-RealWorld-Lite for text-only GRPO and PRA-GRPO.

A plausible explanation is that PRA-GRPO benefits from positive interaction between the two roles: a stronger *Perceiver* provides better visual evidence for the *Reasoner*, while a stronger *Reasoner* can yield more reliable answer-based feedback for training the *Perceiver*. This allows improvements in the two stages to reinforce each other over training.

Case Studies. Figure 7 presents two examples from V-Star that highlight the differences between

Qwen3-VL-Instruct-4B and P2R-4B. In the first, the baseline misses a small but decisive red chair and therefore fails to determine its spatial relation to the road. P2R-4B, by contrast, successfully localizes the chair and correctly infers that it is on the right side of the road. In the second, the baseline attends to the correct bicycle region but fails on the fine-grained detail, misrecognizing its color. P2R-4B instead identifies the bicycle as yellow.

These examples illustrate the complementary roles encouraged by PRA-GRPO. The first example highlights improved localization of relevant evidence, while the second reflects more precise reasoning over localized fine-grained details.

See Appendix E for additional analysis.

5 Conclusion

We propose P2R, a unified framework that decouples perception from reasoning for fine-grained visual reasoning, and PRA-GRPO, a training strategy aligned with this formulation. Built on Qwen3-VL-Instruct models, P2R achieves consistently strong performance across challenging high-resolution fine-grained visual reasoning benchmarks and also improves broader multimodal performance.

Limitations

This work has several limitations. First, although P2R is simple and effective, its two-stage pipeline introduces additional inference cost compared with direct prompting. Second, due to limited computational resources, we have not explored PRA-GRPO at larger training scales, so its full scaling behavior remains unclear. Third, PRA-GRPO relies only on final-answer supervision, which avoids the need for bounding box annotations but also provides a sparse learning signal. Finally, our evaluation mainly focuses on fine-grained visual reasoning and related multimodal benchmarks; broader generalization to interactive or long-horizon settings remains for future work.

Ethics Considerations

This work raises several ethical considerations. First, improving fine-grained visual perception may benefit useful applications, but it could also increase risks in privacy-sensitive settings by enabling models to identify small or sensitive details in high-resolution images. Second, although P2R provides intermediate outputs such as bounding boxes and cropped regions, these should not be interpreted as fully faithful explanations of model decisions. Finally, like other vision-language models, our method may inherit biases and failure modes from its base model and training data, so careful evaluation is needed before deployment in real-world or high-stakes settings.

References

- Shuai Bai, Yuxuan Cai, Ruizhe Chen, Keqin Chen, Xionghui Chen, Zesen Cheng, Lianghao Deng, Wei Ding, Chang Gao, Chunjiang Ge, and 1 others. 2025. Qwen3-vl technical report. *arXiv preprint arXiv:2511.21631*.
- Yan Chen, Long Li, Teng Xi, Long Zeng, and Jingdong Wang. 2025. Perception before reasoning: Two-stage reinforcement learning for visual reasoning in vision-language models. *arXiv preprint arXiv:2509.13031*.
- Yue Fan, Xuehai He, Diji Yang, Kaizhi Zheng, Ching-Chen Kuo, Yuting Zheng, Sravana Jyothi Narayanaraju, Xinze Guan, and Xin Eric Wang. 2025. Grit: Teaching mllms to think with images. *arXiv preprint arXiv:2505.15879*.
- Yuqian Fu, Tinghong Chen, Jiajun Chai, Xihuai Wang, Songjun Tu, Guojun Yin, Wei Lin, Qichao Zhang, Yuanheng Zhu, and Dongbin Zhao. 2025. Srft: A single-stage method with supervised and reinforcement fine-tuning for reasoning. *arXiv preprint arXiv:2506.19767*.
- Daya Guo, Dejian Yang, Haowei Zhang, Junxiao Song, Peiyi Wang, Qihao Zhu, Runxin Xu, Ruoyu Zhang, Shirong Ma, Xiao Bi, and 1 others. 2025. Deepseek-r1: Incentivizing reasoning capability in llms via reinforcement learning. *arXiv preprint arXiv:2501.12948*.
- Jack Hong, Chenxiao Zhao, ChengLin Zhu, Weiheng Lu, Guohai Xu, and Xing Yu. 2025. Deepeyesv2: Toward agentic multimodal model. *arXiv preprint arXiv:2511.05271*.
- Yushi Hu, Weijia Shi, Xingyu Fu, Dan Roth, Mari Ostendorf, Luke Zettlemoyer, Noah A Smith, and Ranjay Krishna. 2024. Visual sketchpad: Sketching as a visual chain of thought for multimodal language models. *Advances in Neural Information Processing Systems*, 37:139348–139379.
- Wenxuan Huang, Bohan Jia, Zijie Zhai, Shaosheng Cao, Zheyu Ye, Fei Zhao, Zhe Xu, Yao Hu, and Shaohui Lin. 2025. Vision-r1: Incentivizing reasoning capability in multimodal large language models. *arXiv preprint arXiv:2503.06749*.
- Aaron Hurst, Adam Lerer, Adam P Goucher, Adam Perelman, Aditya Ramesh, Aidan Clark, AJ Ostrow, Akila Welihinda, Alan Hayes, Alec Radford, and 1 others. 2024. Gpt-4o system card. *arXiv preprint arXiv:2410.21276*.
- Mahyar Khayatkhoei, Prateek Chhikara, Filip Ilievski, and 1 others. 2025. Mllms know where to look: Training-free perception of small visual details with multimodal llms. In *International Conference on Learning Representations*, volume 2025, pages 68194–68213.
- Solomon Kullback. 1951. Kullback-leibler divergence. *Tech. Rep.*
- Woosuk Kwon, Zhuohan Li, Siyuan Zhuang, Ying Sheng, Lianmin Zheng, Cody Hao Yu, Joseph Gonzalez, Hao Zhang, and Ion Stoica. 2023. Efficient memory management for large language model serving with pagedattention. In *Proceedings of the 29th symposium on operating systems principles*, pages 611–626.
- Xin Lai, Junyi Li, Wei Li, Tao Liu, Tianjian Li, and Hengshuang Zhao. 2025. Mini-o3: Scaling up reasoning patterns and interaction turns for visual search. *arXiv preprint arXiv:2509.07969*.
- Xin Lai, Zhuotao Tian, Yukang Chen, Yanwei Li, Yuhui Yuan, Shu Liu, and Jiaya Jia. 2024. Lisa: Reasoning segmentation via large language model. In *Proceedings of the IEEE/CVF conference on computer vision and pattern recognition*, pages 9579–9589.

- Dingming Li, Hongxing Li, Zixuan Wang, Yuchen Yan, Hang Zhang, Siqi Chen, Guiyang Hou, Shengpei Jiang, Wenqi Zhang, Yongliang Shen, and 1 others. 2025a. Viewspatial-bench: Evaluating multi-perspective spatial localization in vision-language models. *arXiv preprint arXiv:2505.21500*.
- Geng Li, Jinglin Xu, Yunzhen Zhao, and Yuxin Peng. 2025b. Dyfo: A training-free dynamic focus visual search for enhancing llms in fine-grained visual understanding. In *Proceedings of the Computer Vision and Pattern Recognition Conference*, pages 9098–9108.
- Haobin Li, Yutong Yang, Yijie Lin, Xiang Dai, Mouxing Yang, and Xi Peng. 2026. Reliable thinking with images. *arXiv preprint arXiv:2602.12916*.
- Hongxing Li, Dingming Li, Zixuan Wang, Yuchen Yan, Hang Wu, Wenqi Zhang, Yongliang Shen, Weiming Lu, Jun Xiao, and Yueting Zhuang. 2025c. Spatialladder: Progressive training for spatial reasoning in vision-language models. *arXiv preprint arXiv:2510.08531*.
- Peng Liu, Haozhan Shen, Chunxin Fang, Zhicheng Sun, Jiajia Liao, and Tiancheng Zhao. 2025a. Vlmfo1: Bridging the gap between high-level reasoning and fine-grained perception in vlms. *arXiv preprint arXiv:2509.25916*.
- Shih-Yang Liu, Xin Dong, Ximing Lu, Shizhe Diao, Peter Belcak, Mingjie Liu, Min-Hung Chen, Hongxu Yin, Yu-Chiang Frank Wang, Kwang-Ting Cheng, and 1 others. 2026. Gdpo: Group reward-decoupled normalization policy optimization for multi-reward rl optimization. *arXiv preprint arXiv:2601.05242*.
- Xianjie Liu, Yiman Hu, Yixiong Zou, Liang Wu, Jian Xu, and Bo Zheng. 2025b. Hide: Rethinking the zoom-in method in high resolution mllms via hierarchical decoupling. *arXiv preprint arXiv:2510.00054*.
- Yuqi Liu, Bohao Peng, Zhisheng Zhong, Zihao Yue, Fanbin Lu, Bei Yu, and Jiaya Jia. 2025c. Seg-zero: Reasoning-chain guided segmentation via cognitive reinforcement. *arXiv preprint arXiv:2503.06520*.
- Zichen Liu, Changyu Chen, Wenjun Li, Penghui Qi, Tianyu Pang, Chao Du, Wee Sun Lee, and Min Lin. 2025d. Understanding r1-zero-like training: A critical perspective. *arXiv preprint arXiv:2503.20783*.
- Ziyu Liu, Zeyi Sun, Yuhang Zang, Xiaoyi Dong, Yuhang Cao, Haodong Duan, Dahua Lin, and Jiaqi Wang. 2025e. Visual-rft: Visual reinforcement fine-tuning. *arXiv preprint arXiv:2503.01785*.
- Zuyan Liu, Yuhao Dong, Yongming Rao, Jie Zhou, and Jiwen Lu. 2024. Chain-of-spot: Interactive reasoning improves large vision-language models. *arXiv preprint arXiv:2403.12966*.
- Fanqing Meng, Lingxiao Du, Zongkai Liu, Zhixiang Zhou, Quanfeng Lu, Daocheng Fu, Botian Shi, Wenhai Wang, Junjun He, Kaipeng Zhang, and 1 others. 2025. Mm-eureka: Exploring visual aha moment with rule-based large-scale reinforcement learning. *CoRR*.
- OpenAI. 2025. [Thinking with images](#).
- John Schulman, Filip Wolski, Prafulla Dhariwal, Alec Radford, and Oleg Klimov. 2017. Proximal policy optimization algorithms. *arXiv preprint arXiv:1707.06347*.
- Hao Shao, Shengju Qian, Han Xiao, Guanglu Song, Zhuofan Zong, Letian Wang, Yu Liu, and Hongsheng Li. 2024a. Visual cot: Advancing multimodal language models with a comprehensive dataset and benchmark for chain-of-thought reasoning. *Advances in Neural Information Processing Systems*, 37:8612–8642.
- Zhihong Shao, Peiyi Wang, Qihao Zhu, Runxin Xu, Junxiao Song, Xiao Bi, Haowei Zhang, Mingchuan Zhang, YK Li, Yang Wu, and 1 others. 2024b. Deepseekmath: Pushing the limits of mathematical reasoning in open language models. *arXiv preprint arXiv:2402.03300*.
- Haozhan Shen, Peng Liu, Jingcheng Li, Chunxin Fang, Yibo Ma, Jiajia Liao, Qiaoli Shen, Zilun Zhang, Kangjia Zhao, Qianqian Zhang, and 1 others. 2025a. Vlm-r1: A stable and generalizable r1-style large vision-language model. *arXiv preprint arXiv:2504.07615*.
- Haozhan Shen, Kangjia Zhao, Tiancheng Zhao, Ruochen Xu, Zilun Zhang, Mingwei Zhu, and Jianwei Yin. 2025b. Zoomeye: Enhancing multimodal llms with human-like zooming capabilities through tree-based image exploration. In *Proceedings of the 2025 Conference on Empirical Methods in Natural Language Processing*, pages 6613–6629.
- Guangming Sheng, Chi Zhang, Zilingfeng Ye, Xibin Wu, Wang Zhang, Ru Zhang, Yanghua Peng, Haibin Lin, and Chuan Wu. 2025. Hybridflow: A flexible and efficient rlhf framework. In *Proceedings of the Twentieth European Conference on Computer Systems*, pages 1279–1297.
- Xinyu Tang, Yuliang Zhan, Zhixun Li, Wayne Xin Zhao, Zhenduo Zhang, Zujie Wen, Zhiqiang Zhang, and Jun Zhou. 2025. Rethinking sample polarity in reinforcement learning with verifiable rewards. *arXiv preprint arXiv:2512.21625*.
- Chaoyang Wang, Kaituo Feng, Dongyang Chen, Zhongyu Wang, Zhixun Li, Sicheng Gao, Meng Meng, Xu Zhou, Manyuan Zhang, Yuzhang Shang, and 1 others. 2025a. Adatooler-v: Adaptive tool-use for images and videos. *arXiv preprint arXiv:2512.16918*.
- Haochen Wang, Yuhao Wang, Tao Zhang, Yikang Zhou, Yanwei Li, Jiacong Wang, Jiani Zheng, Ye Tian, Jiahao Meng, Zilong Huang, and 1 others. 2025b. Grasp any region: Towards precise, contextual pixel understanding for multimodal llms. *arXiv preprint arXiv:2510.18876*.

- Haozhe Wang, Chao Qu, Zuming Huang, Wei Chu, Fangzhen Lin, and Wenhui Chen. 2026. V1-rethinker: Incentivizing self-reflection of vision-language models with reinforcement learning. *Advances in Neural Information Processing Systems*, 38:30865–30891.
- Haozhe Wang, Alex Su, Weiming Ren, Fangzhen Lin, and Wenhui Chen. 2025c. Pixel reasoner: Incentivizing pixel-space reasoning with curiosity-driven reinforcement learning. *arXiv preprint arXiv:2505.15966*.
- Wenbin Wang, Liang Ding, Minyan Zeng, Xiabin Zhou, Li Shen, Yong Luo, Wei Yu, and Dacheng Tao. 2025d. Divide, conquer and combine: A training-free framework for high-resolution image perception in multimodal large language models. In *Proceedings of the AAAI Conference on Artificial Intelligence*, volume 39, pages 7907–7915.
- Zixuan Wang, Dingming Li, Hongxing Li, Shuo Chen, Yuchen Yan, Wenqi Zhang, Yongliang Shen, Weiming Lu, Jun Xiao, and Yueting Zhuang. 2025e. Omninar: Benchmarking agent reasoning in embodied tasks. *arXiv preprint arXiv:2508.05614*.
- Jason Wei, Xuezhi Wang, Dale Schuurmans, Maarten Bosma, Fei Xia, Ed Chi, Quoc V Le, Denny Zhou, and 1 others. 2022. Chain-of-thought prompting elicits reasoning in large language models. *Advances in neural information processing systems*, 35:24824–24837.
- Lai Wei, Liangbo He, Jun Lan, Lingzhong Dong, Yutong Cai, Siyuan Li, Huijia Zhu, Weiqiang Wang, Linghe Kong, Yue Wang, and 1 others. 2026. Zooming without zooming: Region-to-image distillation for fine-grained multimodal perception. *arXiv preprint arXiv:2602.11858*.
- Penghao Wu and Saining Xie. 2024. V?: Guided visual search as a core mechanism in multimodal llms. In *Proceedings of the IEEE/CVF Conference on Computer Vision and Pattern Recognition*, pages 13084–13094.
- Jianhao Yan, Yafu Li, Zican Hu, Zhi Wang, Ganqu Cui, Xiaoye Qu, Yu Cheng, and Yue Zhang. 2026. Learning to reason under off-policy guidance. *Advances in Neural Information Processing Systems*, 38:117157–117186.
- Yi Yang, Xiaoxuan He, Hongkun Pan, Xiyan Jiang, Yan Deng, Xingtao Yang, Haoyu Lu, Dacheng Yin, Fengyun Rao, Minfeng Zhu, and 1 others. 2025. R1-onevision: Advancing generalized multimodal reasoning through cross-modal formalization. *arXiv preprint arXiv:2503.10615*.
- En Yu, Kangheng Lin, Liang Zhao, Jisheng Yin, Yana Wei, Yuang Peng, Haoran Wei, Jianjian Sun, Chunrui Han, Zheng Ge, and 1 others. 2025a. Perception-r1: Pioneering perception policy with reinforcement learning. *arXiv preprint arXiv:2504.07954*.
- Qiyang Yu, Zheng Zhang, Ruofei Zhu, Yufeng Yuan, Xiaochen Zuo, Yu Yue, Weinan Dai, Tiantian Fan, Gaohong Liu, Lingjun Liu, and 1 others. 2026. Dapo: An open-source llm reinforcement learning system at scale. *Advances in Neural Information Processing Systems*, 38:113222–113244.
- Xuan Yu, Dayan Guan, and Yanfeng Gu. 2025b. Zoom-refine: Boosting high-resolution multimodal understanding via localized zoom and self-refinement. *arXiv preprint arXiv:2506.01663*.
- Yi-Fan Zhang, Xingyu Lu, Shukang Yin, Chaoyou Fu, Wei Chen, Xiao Hu, Bin Wen, Kaiyu Jiang, Changyi Liu, Tianke Zhang, and 1 others. 2025. Thyme: Think beyond images. *arXiv preprint arXiv:2508.11630*.
- Yi-Fan Zhang, Huanyu Zhang, Haochen Tian, Chaoyou Fu, Shuangqing Zhang, Junfei Wu, Feng Li, Kun Wang, Qingsong Wen, Zhang Zhang, and 1 others. 2024. Mme-realworld: Could your multimodal llm challenge high-resolution real-world scenarios that are difficult for humans? *arXiv preprint arXiv:2408.13257*.
- Shitian Zhao, Shaoheng Lin, Ming Li, Haoquan Zhang, Wenshuo Peng, Kaipeng Zhang, and Chen Wei. 2026. Pyvision-rl: Forging open agentic vision models via rl. *arXiv preprint arXiv:2602.20739*.
- Shitian Zhao, Haoquan Zhang, Shaoheng Lin, Ming Li, Qilong Wu, Kaipeng Zhang, and Chen Wei. 2025. Pyvision: Agentic vision with dynamic tooling. *arXiv preprint arXiv:2507.07998*.
- Chujie Zheng, Shixuan Liu, Mingze Li, Xiong-Hui Chen, Bowen Yu, Chang Gao, Kai Dang, Yuqiong Liu, Rui Men, An Yang, and 1 others. 2025a. Group sequence policy optimization. *arXiv preprint arXiv:2507.18071*.
- Ziwei Zheng, Michael Yang, Jack Hong, Chenxiao Zhao, Guohai Xu, Le Yang, Chao Shen, and Xing Yu. 2025b. Deepeyes: Incentivizing "thinking with images" via reinforcement learning. *arXiv preprint arXiv:2505.14362*.

A Diagnostic Study

Method	V-Star		
	Attr	Spatial	Overall
<i>Qwen3-VL-4B</i>			
+ Direct CoT	79.1	85.5	81.7
+ Oracle Hint	87.8	94.7	90.6

Table 5: Diagnostic study on V-Star using Qwen3-VL-4B. *Direct CoT* uses only the input image, while *Oracle Hint* additionally provides ground-truth bounding boxes and cropped regions.

We conduct a simple diagnostic study on V-Star (Wu and Xie, 2024) to probe a key question behind this work: is fine-grained visual reasoning limited more by reasoning or by perception? Using Qwen3-VL-4B, we compare a standard Direct CoT setting with an *Oracle Hint* setting that provides ground-truth bounding boxes from the official V-Star annotation file, together with the corresponding cropped regions. Table 5 shows that Oracle Hint improves overall accuracy from 81.7% to 90.6%, with consistent gains on both attribute and spatial questions. The result suggests that many failures are caused not by the inability to reason over evidence, but by the inability to first find the right evidence to reason over.

B Methodology Details

B.1 P2R Inference Details

P2R inference consists of a Perceiver stage for localizing question-relevant evidence and a Reasoner stage for answering based on the localized evidence. We use the following prompts.

Prompt for Perceiver

System Prompt: “You are a helpful assistant.”
User Prompt: $\{question\}$ + “Please carefully observe the image first to identify the object(s) referred to in the question. Note that each object type appears only once in the image. Then provide the 2D bounding box coordinates and labels of the related objects in JSON format.”

Prompt for Reasoner

System Prompt: “You are a helpful assistant.”
User Prompt: $\{question\}$ + “The key visual regions have been highlighted and cropped for you. Think step by step.”

The predicted boxes are highlighted on the original image and cropped into local patches. Both

the highlighted image and the local crops are then provided to the Reasoner.

B.2 PRA-GRPO Details

Algorithm 1 presents the training procedure of PRA-GRPO. Training alternates between Perceiver and Reasoner phases. In each phase, the active role is optimized while the other role is frozen using the checkpoint from the previous stage. For each training sample, we draw a group of rollouts from the active role, compute binary rewards from final-answer correctness, and derive group-relative advantages under GRPO. The resulting objective is then used to update only the active role.

The predicted bounding boxes are parsed from the model outputs using regular expressions. During post-processing, to keep the visual context within the input limit, we do not restrict the number of boxes rendered on the original image, but crop local patches from only the first three predicted boxes.

Algorithm 1 PRA-GRPO

Require: Perceiver π_p , Reasoner π_r , dataset \mathcal{D} , group size G , stage schedule

- 1: **for** each iteration **do**
- 2: Sample a mini-batch (I, Q, Y) from \mathcal{D}
- 3: Select the active role $\phi \in \{p, r\}$ by the schedule
- 4: Load the previous-stage checkpoint for the other role
- 5: *// Step 1: Role-aware rollout*
- 6: **for** each (I, Q, Y) in the mini-batch **do**
- 7: **if** $\phi = p$ **then**
- 8: Set $x \leftarrow (I, \mathcal{T}_p(Q))$
- 9: Sample $\{\mathcal{B}_i\}_{i=1}^G \sim \pi_p(\cdot | x)$
- 10: **for** $i = 1, \dots, G$ **do**
- 11: Derive (I_a^i, I_c^i) from \mathcal{B}_i
- 12: Use the frozen Reasoner to obtain Y_i
- 13: Set $o_i \leftarrow \mathcal{B}_i$
- 14: **end for**
- 15: **else**
- 16: Obtain \mathcal{B} from the frozen Perceiver
- 17: Derive (I_a, I_c) from \mathcal{B}
- 18: Set $x \leftarrow (I_a, I_c, Q)$
- 19: Sample $\{Y_i\}_{i=1}^G \sim \pi_r(\cdot | x)$
- 20: **for** $i = 1, \dots, G$ **do**
- 21: Set $o_i \leftarrow Y_i$
- 22: **end for**
- 23: **end if**
- 24: *// Step 2: Reward computation*
- 25: **for** $i = 1, \dots, G$ **do**
- 26: Compute reward $r_i \leftarrow \mathbb{I}[Y_i = Y]$
- 27: **end for**
- 28: *// Step 3: Group-relative advantage*
- 29: Compute $\mu \leftarrow \text{mean}(\{r_i\})$, $\sigma \leftarrow \text{std}(\{r_i\})$
- 30: **for** $i = 1, \dots, G$ **do**
- 31: Compute $A_i \leftarrow (r_i - \mu)/(\sigma + \epsilon)$
- 32: **end for**
- 33: *// Step 4: GRPO policy update*
- 34: Compute $\mathcal{L}_{\text{GRPO}}$ from $\{o_i, A_i\}_{i=1}^G$
- 35: Update the active role with $\mathcal{L}(\theta) = \mathcal{L}_{\text{GRPO}}(\theta)$
- 36: **end for**
- 37: **end for**

C Training Details

C.1 Training Dataset

We construct a 10K training set by random sampling from three complementary data sources: 3K examples from DeepEyes (Zheng et al., 2025b), 3K from VisualProbe (Lai et al., 2025), and 4K from ZwZ (Wei et al., 2026). These sources provide diverse supervision for fine-grained visual perception and evidence localization, while also covering different difficulty levels: DeepEyes is relatively easier, ZwZ presents medium-difficulty fine-grained perception cases, and VisualProbe is the most challenging due to small targets, cluttered scenes, and many distractors.

- **DeepEyes:** We sample 3K examples from DeepEyes as a relatively easy source of training data. DeepEyes is curated for visually useful evidence and fine-grained perception, with filtering procedures for difficulty, answer validity, and perception utility. This makes it a suitable starting point for learning basic evidence localization behavior.
- **ZwZ:** We sample 4K examples from ZwZ as a medium-difficulty source of fine-grained perception data. ZwZ is synthetically generated by Region-to-Image distillation: strong teacher models first create question-answer pairs on micro-cropped regions, and the supervision is then distilled back to the full image with explicit region grounding. The resulting samples emphasize subtle local details while remaining more controlled than naturally hard search problems.
- **VisualProbe:** We sample 3K examples from VisualProbe as the hardest portion of the training mixture. Built from high-resolution images with very small targets and many distractors, it places strong demands on identifying sparse and localized visual evidence under clutter, making it particularly suitable for training robust perception behavior.

Overall, this mixture provides a coarse-to-hard spectrum of training difficulty, from relatively accessible grounding examples in DeepEyes, to medium-difficulty fine-grained cases in ZwZ, and finally to challenging visual search instances in VisualProbe. Despite using only 10K training examples in total, our method achieves significant

performance gains, highlighting both the effectiveness of the proposed training framework and its strong data efficiency.

C.2 Detailed Training Setup

Table 6 summarizes the main training hyper-parameters. We implement PRA-GRPO using the VeRL (Sheng et al., 2025) framework. The Perceiver and Reasoner share the same training configuration and differ only in the prompt and response length limits. During training, we cap the maximum image resolution at $2048 \times 32 \times 32$ pixels as the image pixel budget.

Parameter	Value
algorithm.adv_estimator	grpo
train_batch_size	64
truncation	error
filter_overlong_prompts	True
rollout.n	8
lr	1×10^{-6}
ppo_mini_batch_size	64
ppo_micro_batch_size_per_gpu	8
use_kl_loss	True
kl_loss_coef	1×10^{-2}
kl_loss_type	low_var_kl
entropy_coef	0
use_kl_in_reward	False
n_gpus_per_node	4
nnodes	1
total_epochs	1
perceiver_max_prompt_length	2560
perceiver_max_response_length	1024
reasoner_max_prompt_length	8704
reasoner_max_response_length	2048

Table 6: Key training hyper-parameters for PRA-GRPO.

D Evaluation Details

D.1 Evaluation Datasets

We evaluate P2R on three benchmark suites used in the main results: V-Star (Wu and Xie, 2024), HR-Bench (4K and 8K) (Wang et al., 2025d), and MME-RealWorld-Lite (Zhang et al., 2024). These benchmarks provide complementary evaluation settings, ranging from high-resolution fine-grained perception to broader real-world multimodal perception and reasoning.

- **V-Star:** V-Star is designed to evaluate multimodal models in challenging visual sce-

narios where the required evidence is difficult to locate. It is built from 191 high-resolution images, with an average resolution of 2246×1582 , and contains two sub-tasks: attribute recognition and spatial relationship reasoning. The questions are manually curated so the correct answer cannot be reliably guessed without accurate visual grounding.

- **HR-Bench:** HR-Bench focuses on fine-grained perception in high-resolution images. It contains two sub-tasks: Fine-grained Single-instance Perception (FSP), which evaluates recognition of detailed attributes such as color and material, and Fine-grained Cross-instance Perception (FCP), which evaluates relative position understanding across objects. Each sub-task contains 100 samples. We report results on both HR-Bench-4K and HR-Bench-8K, corresponding to cropped 4K images and original 8K images, respectively.
- **MME-RealWorld-Lite:** We further evaluate on MME-RealWorld-Lite, a lightweight subset of MME-RealWorld commonly used for efficient evaluation. Following the official lite setting, it contains 50 samples per task, or all samples when a task has fewer than 50 examples. The benchmark covers diverse real-world scenarios, including OCR in the wild, remote sensing, diagrams and tables, autonomous driving, and monitoring, and therefore serves as a broader test of multimodal perception and reasoning beyond the high-resolution benchmarks above.

Together, these benchmarks allow us to evaluate P2R in both fine-grained high-resolution settings and more general real-world multimodal understanding scenarios.

D.2 Detailed Evaluation Setup

For evaluation, we use greedy decoding with temperature 0 to ensure reproducible results. In addition, we increase the maximum image resolution to $4096 \times 32 \times 32$ pixels at evaluation time.

E Additional Analysis

E.1 Additional Training Dynamics

Accuracy on High-Resolution Benchmarks. Figure 9 shows the evaluation accuracy on V-Star, HR-Bench-4K, and HR-Bench-8K across the Perceiver and Reasoner training phases. We observe

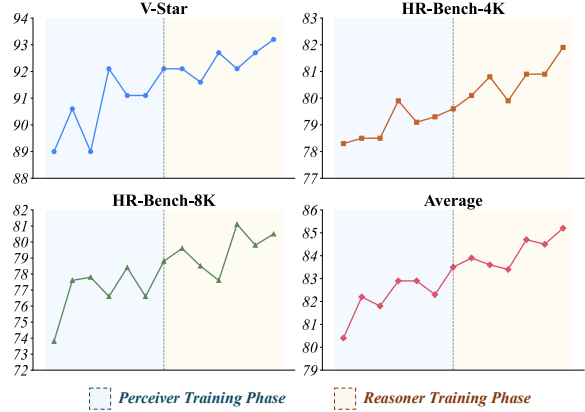


Figure 9: Evaluation accuracy dynamics on high-resolution benchmarks during the Perceiver and Reasoner training phases of PRA-GRPO.

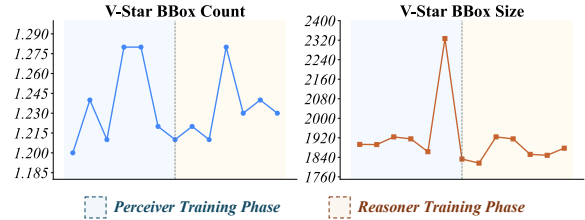


Figure 10: Dynamics of bounding box count and size on V-Star during the Perceiver and Reasoner training phases of PRA-GRPO.

consistent gains on all three benchmarks, with average performance steadily improving throughout training. This result suggests that both stages of PRA-GRPO contribute to better fine-grained visual perception on challenging high-resolution images. In particular, the gains continue not only during the Perceiver phase, where the model directly learns to localize informative evidence, but also during the Reasoner phase, indicating that improving downstream reasoning can further enhance the overall perceive-to-reason pipeline.

Statistics of Bounding Box Count and Size.

Figure 10 plots the average bounding box count and size on V-Star throughout training. Importantly, we do not observe a monotonic increase in either the number of predicted boxes or their spatial extent. This suggests that the model is not exploiting the reward by simply proposing more regions or enlarging boxes to cover as much of the image as possible. Instead, the model remains focused on identifying compact and informative regions that are most relevant to the final answer. At the same time, both statistics exhibit a rise-then-fall pattern, which is consistent with an exploration process: the

model initially explores broader region proposals and then gradually refines them toward more selective and targeted localization. Interestingly, these box statistics also change during the Reasoner training phase. Although only the Reasoner is updated in that stage, its improvement still affects the overall role interaction in PRA-GRPO, which in turn influences the Perceiver’s learned bounding-box behavior in the final pipeline.

E.2 Efficiency Analysis

Figure 11 compares throughput and average performance on the high-resolution benchmarks. Overall, P2R achieves a favorable efficiency-accuracy trade-off: compared with the corresponding Qwen3-VL-Instruct base models, P2R substantially improves benchmark performance while retaining relatively high inference efficiency. The official tool-use baseline follows the *Thinking with Images* paradigm, and P2R is both more accurate and much faster than this variant. Although P2R is slower than the base models due to the additional interaction, it remains practical in terms of inference cost.

For fairness, we do not include direct efficiency comparisons with visual search methods. Our experiments use a unified vLLM (Kwon et al., 2023) backend, whereas visual search methods typically rely on more complex multi-stage pipelines and often use different backends. Direct wall-clock comparisons would therefore be confounded by implementation differences. Still, prior work (Liu et al., 2025b; Yu et al., 2025b) suggests that visual search methods usually incur much higher latency; for example, methods such as ZoomEye (Shen et al., 2025b) are often reported to require more than $5\times$ the inference time of the underlying base model. This further suggests that P2R offers a more favorable practical efficiency-performance trade-off.

E.3 Analysis of Bounding Box Quality

Figure 12 highlights the importance of bounding boxes in our framework. Compared with the no-bounding-box setting, using bounding boxes leads to substantial performance gains, showing that explicitly focusing on relevant regions is critical for fine-grained visual reasoning. This confirms the importance of decoupling perception and reasoning in the P2R framework. In contrast, random bounding boxes hurt performance, further showing that accurate region localization is essential.

After PRA-GRPO training, the model’s self-generated bounding boxes already achieve perfor-

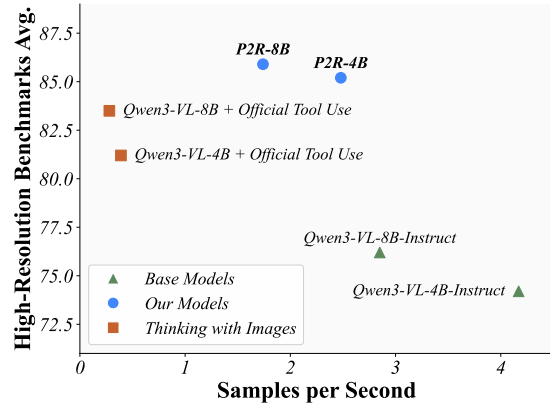


Figure 11: Comparison of inference throughput (samples per second) and average accuracy on the high-resolution benchmarks for Qwen3-VL-Instruct, P2R, and Qwen3-VL with official tool use. Official tool use denotes the released tool-calling inference pipeline of Qwen3-VL, which follows a *Thinking with Images* style of interaction.

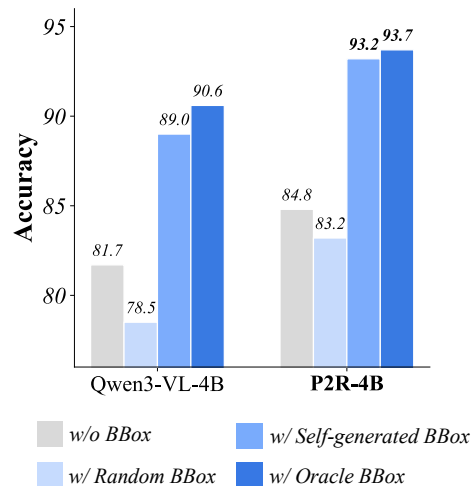


Figure 12: Comparison of different bounding box inputs on V-Star for Qwen3-VL-4B and P2R-4B.

mance very close to that of ground-truth bounding boxes. For P2R-4B, the gap between self-generated and oracle boxes is only 0.5% (93.2% vs. 93.7%), indicating that the learned Perceiver can accurately identify key regions without external box supervision at inference time. In addition, P2R-4B is more robust to random bounding boxes than the base model, with a much smaller degradation under noisy box inputs. This suggests that PRA-GRPO improves both region localization quality and robustness to imperfect visual hints.

E.4 GRPO vs. DAPO

DAPO (Yu et al., 2026) is an improved variant of GRPO (Schulman et al., 2017; Liu et al., 2025d;

Yan et al., 2026; Zheng et al., 2025a; Fu et al., 2025) that has shown strong performance on mathematical reasoning tasks. Compared with standard GRPO, DAPO introduces several modifications, including removing the KL divergence term, clip-higher, dynamic sampling, token-level policy gradient loss, and overlong reward shaping. Prior work (Tang et al., 2025; Liu et al., 2026) has shown that these changes can lead to clear gains over GRPO on text-based reasoning benchmarks, and recent work (Lai et al., 2025; Wei et al., 2026) on fine-grained visual perception has also adopted this training recipe.

However, in our setting, we find that DAPO is less suitable for training the Perceiver. In particular, during the Perceiver phase, DAPO causes the predicted bounding box count to drop rapidly and quickly converge to one. This behavior is problematic for tasks that require multiple boxes. For example, many samples in the spatial relationship reasoning split of V-Star require comparing the relative positions of two objects. If the model outputs only a single bounding box, it cannot reliably capture both objects, leading to a clear performance drop. On the 4B model, DAPO achieves only 85.8% on V-Star Spatial, whereas GRPO reaches 94.7%.

We hypothesize that this issue is related to the removal of the KL divergence term in DAPO. Without KL regularization, the policy can more easily drift away from the original response pattern and collapse to a simpler mode that generates only one bounding box. While such behavior may not be problematic in pure text reasoning, it is harmful in our setting, where the model must maintain flexible multi-box perception behavior. We therefore use GRPO instead of DAPO in all main experiments.

E.5 More Cases

Figures 13, 14, 15, 16, 17, and 18 show additional successful cases of P2R-4B across diverse benchmarks and task types, including fine-grained attribute recognition, spatial relation reasoning, chart understanding, remote sensing perception, and OCR-intensive reasoning. Overall, these examples exhibit a consistent perceive-to-reason pattern: the model first identifies a compact region relevant to the query, and then uses the zoomed-in crop to extract fine-grained evidence for the final answer. This behavior is particularly useful when the target evidence is small, subtle, or embedded in cluttered high-resolution scenes. Across these cases, P2R-4B can successfully localize and reason over key

visual evidence such as small symbols, distant objects, fine-grained text, chart segments, and tiny structures in remote-sensing images.

We also show two representative failure cases in Figures 19 and 20. In Figure 19, the model correctly localizes the clock tower and zooms into the relevant clock face, indicating that the Perceiver identifies the right evidence. The error instead comes from fine-grained visual recognition in the cropped region: the model mistakenly interprets the hour hand as pointing to 12 rather than 11, which leads to the wrong answer. This example suggests that even with accurate localization, P2R-4B can still fail on subtle visual reading tasks that require precise interpretation of small details.

In Figure 20, the model also successfully detects the river, but the selected box covers only part of the river rather than the full river region on the left side of the image. As a result, the cropped evidence does not fully preserve the spatial context needed to distinguish whether the answer should be “left” or “upper.” This incomplete localization introduces ambiguity in the reasoning stage. If the full left-side river region were captured, this ambiguity would likely be avoided. This case highlights that, beyond finding the relevant object, the spatial extent of the selected region is also crucial for correct downstream reasoning.



What kind of animal is on the blue sail?

(A) spider

(B) Dog

(C) fish

(D) bird

```
``json [
```

```
  {"bbox_2d": [305, 300, 316, 364], "label": "spider on blue sail"}
```

```
] ``
```



Looking at the first image, I can see a sailboat with a large blue sail in the middle-left portion of the scene. **There is a red box highlighting a specific area on this blue sail.**

When I look at **the second, zoomed-in image**, I can clearly see the shape on the blue sail. **It has eight legs and a body, which is characteristic of a spider.**

The shape is also very similar to the logo of the "Spider" sailboat class, which is known for its distinctive spider emblem.

Therefore, **the animal on the blue sail is a spider.** ✓

Figure 13: A successful case of P2R-4B on the V-Star Attribute.



Is the seesaw on the left or right side of the red vehicle?

(A) right

(B) left

```
```json [
 {"bbox_2d": [817, 546, 839, 587], "label": "red vehicle"},
 {"bbox_2d": [879, 633, 944, 750], "label": "seesaw"}
] ```
```



Looking at the first image, I can see the red vehicle parked in the garage on the left side of the road.

The playground equipment, including the seesaw, is located to the right of the road, further to the right of the vehicle.

**In the second and third images, which are close-ups of the area, the seesaw is clearly visible on the right side of the frame, while the red car is on the left side of the frame.**

**The seesaw is on the right side of the red vehicle. ✓**

Figure 14: A successful case of P2R-4B on the V-Star Spatial.



What is written on the white board in front of the girl in purple shorts?

- (A) ELVTE
- (B) ELEVATE
- (C) CeVaY
- (D) ELEVATE

```
``json [
 {"bbox_2d": [372, 580, 436, 623],
 "label": "white board with text ELEVATE"}
]
```





Looking at the first image, **there is a white rectangular board placed on the grass in front of the girl wearing purple shorts.** The board has text printed on it.

**In the second, zoomed-in image, the text is clearly legible. It reads "ELE VATE" with the 'V' stylized or possibly part of a logo. The full word appears to be "ELEVATE".**

Among the options provided, "ELEVATE" matches this observation exactly. Option A "ELVTE" is incorrect as it's misspelled and doesn't match the actual text. Option C "CeVaY" is not present. Option D "ELEVATE." includes a period which is not present in the text on the board.

Therefore, **the correct answer is B.** ✓

Figure 15: A successful case of P2R-4B on the HR-Bench FSP.


  Where is the structure of blue, yellow, and green alternating colors in the picture?


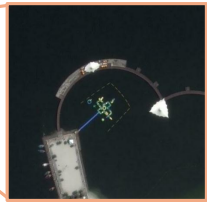
(A) In the lower right corner of the picture.  
 (B) At the bottom left of the picture .  
 (C) **Inside the heart-shaped water area at the top left of the picture.**  
 (D) In the upper right corner of the picture.  
 (E) This image doesn't feature the position.


```

 ``json [
 {"bbox_2d": [295, 173, 320, 204],
 "label": "structure of blue, yellow, and green alternating colors"}
] ``

```



 Looking at the first image, I can see **a red box highlighting a specific area near the water.**

When I examine the **second, zoomed-in image**, I can clearly see **a structure with blue, yellow, and green alternating colors located inside the heart-shaped water area at the top left of the picture.**

**This matches option C. ✓**

Figure 16: A successful case of P2R-4B on the MME-RealWorld-Lite Perception Remote Sensing.



'Which product category has the highest value of Average Revenue by Product', according to the pie chart?



- (A) **Membership Revenue**
- (B) Court Rentals
- (C) Day Rate Revenue
- (D) Service Revenue
- (E) The image does not feature the number.

```

""json [
 {"bbox_2d": [445, 697, 620, 928],
 "label": "Pie chart showing Average Revenue by Product with labeled segments"}
] ""

```



Looking at the pie chart titled "Average Revenue by Product", I need to identify which segment is the largest. The chart is divided into several colored sections, each labeled with a product category and its percentage.

- The segments are:
- **Membership Revenue: 34%**
  - **Other Income: 22%**
  - **Product Revenue: 23%**
  - **Court Rentals: 11%**
  - **Day Rate Revenue: 6%**

By comparing these percentages, **34% is the highest value. The category associated with 34% is "Membership Revenue".**

Therefore, **the product category with the highest value of Average Revenue by Product' is Membership Revenue.** ✓

Figure 17: A successful case of P2R-4B on the MME-RealWorld-Lite Reasoning Diagram and Table.



What time is it now?

- (A) 10:18.
- (B) 12:00.**
- (C) 11:00.
- (D) 15:00.
- (E) The image does not feature the related information.

```

""json [
 {"bbox_2d": [603, 174, 798, 375],
 "label": "digital display showing map and time"}] ""

```



**Looking at the second image, which is a close-up of the car's infotainment screen, I can clearly see the digital clock in the top right corner of the display. The time shown is "12:00".**

**This is also visible in the first image, where the same screen is highlighted with a red box, showing the same time.**

**Therefore, the correct answer is (B) 12:00. ✓**

Figure 18: A successful case of P2R-4B on the MME-RealWorld-Lite Reasoning OCR with Complex Context.



What is the time shown on the clock?

- (A) Approximately 11:00
- (B) Approximately 12:15
- (C) Approximately 12:00
- (D) Approximately 11:10

```
```json [  
  {"bbox_2d": [286, 250, 334, 527], "label": "clock tower"}  
] ```
```



Looking at the close-up image of the clock tower, I can see two large clock faces. The hands on both clocks are positioned very similarly.

On the right clock face, the hour hand is pointing directly at the Roman numeral XII (which represents 12), and the minute hand is also pointing directly at the XII. This indicates that the time is exactly 12:00.

The left clock face shows the same configuration, confirming this reading.

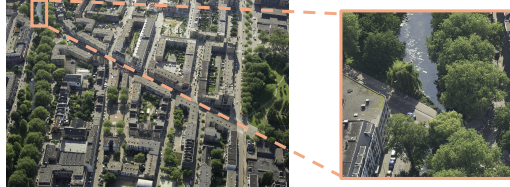
Therefore, the correct answer is C. Approximately 12:00. ❌

Figure 19: A failure case of P2R-4B on the HR-Bench FSP.



Where the river is in the picture?
 (A) In the right area of the picture.
 (B) In the upper right area of the picture.
 (C) In the upper area of the picture.
 (D) **In the left area of the picture.**
 (E) This image doesn't feature the position.

```
```json [
 {"bbox_2d": [97, 0, 143, 138], "label": "river"}
] ```
```



Looking at the first image, I can see a red box highlighting a narrow waterway in the upper left corner. This is clearly a river or canal.

The second image provides a closer view of this same waterway, confirming it is a river flowing between trees and buildings.

Since the river is located in the upper left portion of the first image, and the options refer to "upper area" or "left area", I need to determine which option best describes its location relative to the entire picture.

Option (C) "In the upper area of the picture." would be correct if the river were in the top part of the image, which it is. Option (D) "In the left area of the picture." would also be correct if the river were on the left side, which it is as well. However, since the river is specifically in the upper left corner, both (C) and (D) could be argued.

But looking at the options provided, (C) is more precise because the river is not just on the left side but specifically in the upper part of the image, as seen in the first image where the red box is in the upper left.

Given that the river is in the upper area of the picture, option (C) is the most accurate choice. ❌

Figure 20: A failure case of P2R-4B on the MME-RealWorld-Lite Perception Remote Sensing.